Int. J. Heat Mass Transfer. Vol. 31, No. 9, pp. 1815–1833, 1988
Printed in Great Britain

0017-9310/88 $3.00 + 0.00

Experimental investigation and analytical modeling of a closed two-phase thermosyphon with imposed convection boundary conditions

CLAUDIO CASAROSA
Dipartimento di Energetica, Università di Pisa, Pisa 56100, Italy

and

FLAVIO DOBRAN†
Department of Applied Science, New York University, New York, NY 10003, U.S.A.

(*Received* 3 *December* 1987 *and in final form* 5 *February* 1988)

Abstract—A closed two-phase thermosyphon operating with Refrigerant-11 and with imposed convection boundary conditions at the heated and cooled surfaces is experimentally investigated and analytically modeled with a lumped parameter model for varying working fluid temperatures. The thermosyphon exhibits different operational modes depending on the heating and cooling fluids' temperature difference. An increase of this temperature difference produces at first a maximum heat transfer rate identified with the flooding heat transfer limit. Beyond this limit the thermosyphon operation reverts to a different steady state through a transient non-equilibrium process. The new steady state, identified as the thermal blocking condition, produces a lower heat transfer capacity and is attributed to the simultaneous existence of: (1) a new flooding state near or at the exit of the adiabatic section, and (2) the dryout in the evaporator resulting from the transfer of liquid in the evaporator pool to the condenser during the transient process which leads to the thermal blocking condition. The limiting operational modes of the thermosyphon are modeled by a lumped parameter model that accounts for different geometrical configurations and liquid entrainment in the vapor. A comparison between the predicted and experimental heat transfer rates, prior and during the thermal blocking condition, demonstrates the model's utility to predict complex thermohydrodynamic processes in a thermosyphon.

1. INTRODUCTION

THE ADDITION of heat to a two-phase thermosyphon consisting of a closed vertical tube and operating in a gravity field causes the liquid at the bottom of the tube to evaporate. The vapor rises to the top of the tube where it is condensed, and the condensate returns to the evaporator section by gravity as a falling liquid film. Depending on the level and manner of the heat addition in the evaporator and removal in the condenser, on the geometry of the thermosyphon and on the working fluid characteristics, a thermosyphon may exhibit different operational modes or heat transfer limits [1–13].

The experimental studies which have been conducted with the controlled heat transfer rate to the evaporator show the existence of the dryout limit, the burnout limit, the flooding limit, the oscillation limit and the transition-to-different-flow-regime limit. The *dryout heat transfer limit* occurs when some portion of the evaporator surface ceases to be cooled effectively by the liquid film, whereas the *burnout* or *critical heat transfer limit* occurs in the liquid pool. Both of these heat transfer limits lead to the wall temperature excursions: the former occurs when the amount of working fluid is a minimum for the thermosyphon to have a continuous circulation of vapor and condensate, whereas the latter occurs in the liquid pool and is similar to the critical heat flux condition in pool boiling. The *flooding heat transfer limit* is observed with large liquid fillings in long thermosyphons and at large axial and small radial heat fluxes. This limit occurs due to the instability of the liquid film generated by the high interfacial shear produced by the high vapor velocity induced by high axial heat fluxes. A high vapor shear gives rise to the entrainment of liquid from the film into the vapor core that may be pronounced during the flooding process. When the heat flux is increased above the flooding limit heat flux in a heat transfer controlled situation, it is possible to obtain another limiting operation of the thermosyphon called the *oscillation heat transfer limit* [10, 11]. This is characterized by high working fluid temperature oscillations of the order of 300°C. The oscillations are associated with the liquid film flow reversal, the accumulation of liquid in the condenser, falling of the accumulated liquid due to gravity into the evaporator, establishment of a film flow situation again, and the occurrence of flooding and film flow reversal causing the cycle to repeat itself. These flood-

† Author to whom correspondence should be addressed.

NOMENCLATURE

A	heat transfer area
$A_{ia}, A_{ic}, A_{wa}, A_{wc}$	velocity profile coefficients in the interfacial and wall shear stress equations
B	velocity profile coefficients in equations (9)–(12)
C	specific heat at constant pressure
Ca	capillary number, defined by equations (24)
d_{coil}	external coil diameter in the condenser
D	tube internal diameter, $2R$
E_a, E_c	liquid entrainments in the adiabatic and condenser regions
E	entrainment parameter, defined by equation (29)
f	frictional coefficient
h	heat transfer coefficient
h_h	homogeneous enthalpy in the core
h_{LG}	enthalpy of evaporation
h^*	liquid filling parameter, defined by equation $(30)_2$
g	gravitational constant
k	thermal conductivity
$l; l^*$	thermosyphon length; l/R_a
M	total mass of the working fluid, defined by equation (4)
M_a, M_{c^+}, M_{c^-}	mass flow rate per unit area at sections a, c^+ and c^- in Fig. 7
N_{coil}	number of coil turns
N_{Lc}	two-phase Grashof number, defined by equations (23)
p	pressure
Pr	Prandtl number
q	heat flux rate
$Q; Q^*$	heat transfer rate; heat transfer parameter defined by equation (27)
Q_L	volumetric liquid filling
r	radial coordinate
R	tube radius
Re	Reynolds number
T	temperature
T^*	average temperature of the working fluid
$\tilde{T}$	average temperature of the liquid film
U	axial component of velocity
x	core quality
x_1^*	non-dimensional length, $\tilde{z}/R$
x_2^*	non-dimensional variable, $\tilde{\delta}\tilde{z}/R^2$
$\tilde{z}$	length specified in Fig. 7.

Greek symbols

α	core void fraction
Γ	mass flow rate per unit tube periphery
$\tilde{\delta}$	average film thickness, see Fig. 7
$\mu; \mu^*$	viscosity; μ_G/μ_L
$\rho; \rho^*$	density; ρ_G/ρ_L
σ	surface tension
τ	shear stress.

Subscripts

a	adiabatic region or section a in Fig. 7
c	condenser region or section c in Fig. 7
G	vapor
$G\tilde{z}_a$	vapor-averaged over $\tilde{z}_a$
$G\tilde{z}_c$	vapor-averaged over $\tilde{z}_c$
h	homogeneous
i	interface
l	laminar
L	liquid
p	liquid pool
sat	saturation condition
t	top of the thermosyphon
w	tube wall
1	heating fluid inlet
2	cooling fluid inlet.

ing-triggered flow oscillations are observed for liquid fillings of about one third. For small and large liquid fillings these oscillations apparently do not occur, but instead the thermosyphon operation is shifted to different steady states at lower or higher pressures. The heat transfer limits associated with these flow regime changes are not well understood to date and may be called the *transition-to-different-flow-regime heat transfer limits.*

The operation of a thermosyphon at imposed heating and cooling fluid temperatures or convection boundary conditions allows for the control of the evaporator surface temperature and, therefore, does not readily produce the destruction or burnout of the heat transfer surface. Instead, the thermosyphon operation may be limited by the thermal blocking heat transfer limit [12] when an attempt is made to increase the temperature difference between the heating and cooling fluids beyond that which produces the maximum heat transfer rate. Experiments which were conducted on a thermosyphon as described in ref. [12] demonstrate that the thermal blocking heat transfer limits are lower than the maximum heat transfer limits associated with flooding, and are independent of the subsequent increase of the temperature difference between the heating and cooling fluids.

The purpose of this paper is to present the results of the more extensive experimental investigations than reported in the previous work [12]. These experiments were conducted on a closed two-phase thermosyphon with imposed heating and cooling fluid temperatures where the heat transfer is limited by the thermal block-

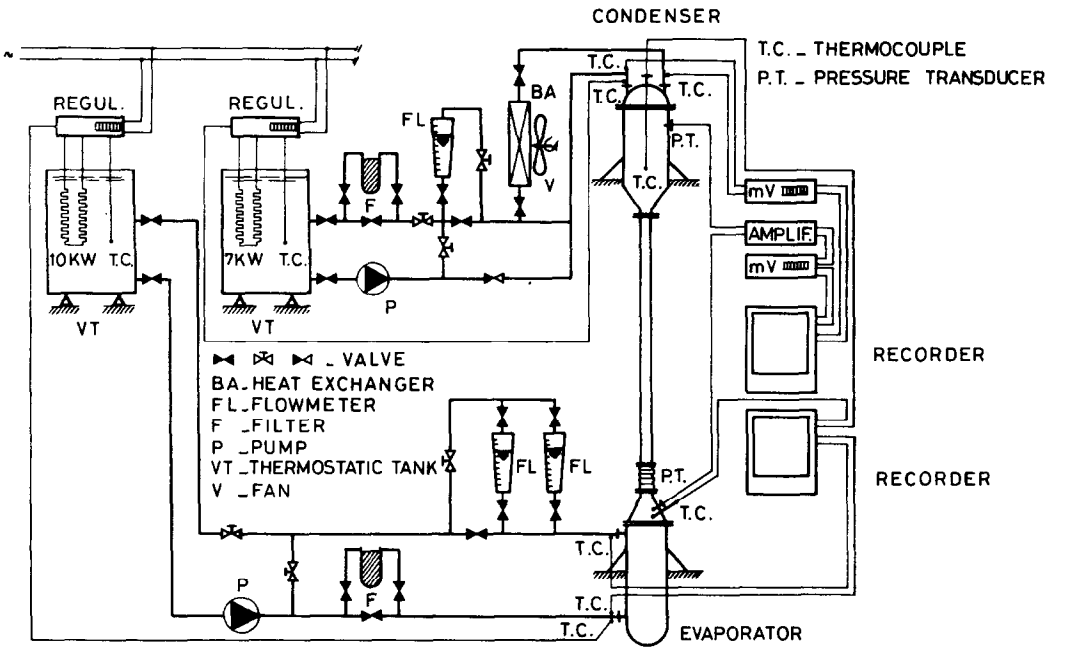

FIG. 1. Schematic of the experimental apparatus.

ing heat transfer limit. Moreover, in an attempt to explain the steady-state conditions in the thermosyphon, prior and during the thermal blocking, an analytical model is also presented and shown that it may be used to explain the limiting heat transfer rates of the thermosyphon at different operating temperatures.

2. EXPERIMENTAL STUDIES

2.1. *Description of the experimental apparatus*

The experimental studies of the heat transfer processes in a closed two-phase flow thermosyphon were conducted with an experimental facility as illustrated in Fig. 1, and with a thermosyphon design as shown in Fig. 2. The thermosyphon was designed for applications to the geothermal systems and its working fluid is Refrigerant-11 with a filling charge of 0.006 m^3. The evaporator section consists of a shell-and-tube heat exchanger with the heating fluid (water) flowing through the shell side. The heat transfer area of the evaporator is 1.45 m^2 and its length and internal diameter are 1.4 and 0.168 m, respectively. The evaporator is connected to the adiabatic region by means of a truncated-cone section. The adiabatic section has an internal diameter of 0.032 m and a length of 3.62 m. The connection between the adiabatic region and the condenser of the thermosyphon is also achieved by means of a truncated-cone section. The condenser length is 0.54 m and its internal shell diameter is 0.206 m. The vapor condensation within the condenser is achieved with two helical coils with a heat transfer area of 0.53 m^2, utilizing water as the cooling medium.

As illustrated in Fig. 1, the heating and cooling water temperatures of the evaporator and condenser are independently controllable. Each heating and cooling loop consists of flow and temperature measuring stations for the determination of the heating and cooling heat transfer loads. The accuracy of flow measurement is estimated to be $\pm 2\%$; that of the heating and cooling fluid temperature differences within $\pm 0.1°C$, giving an accuracy of $\pm 5\%$ in the heat transfer rate after accounting for thermal leaks. The temperature of the working fluid in the thermosyphon can be measured at two different stations:

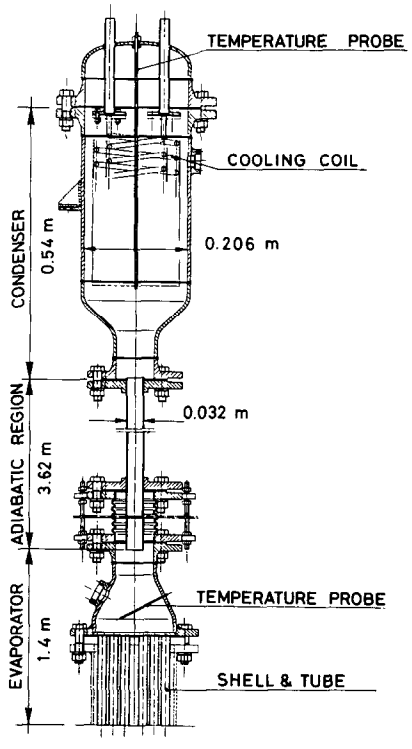

FIG. 2. Design details of the experimental thermosyphon.

one just above the tubes in the evaporator, and the other along the axis of the cooling coil in the condenser (Fig. 2). The moving thermocouple probe in the condenser allows for the identification and purging of the non-condensable gases in the thermosyphon. The pressure difference of the refrigerant between the evaporator and condenser sections can be measured by two absolute pressure transducers with an accuracy of $\pm 10\%$ at the lowest pressures, and $\pm 1\%$ at the highest pressures during the thermal blocking conditions.

During the early phase of experimentation, a thermosyphon of a design similar to that shown in Fig. 2 was used [13], except with the controlled heat transfer rate in the evaporator, and constructed with a transparent adiabatic section for the flow visualization, to obtain some experience with the experimental facility. These preliminary experiments showed that the working fluid temperature remains almost constant and that it is not a good indication of the thermohydrodynamic processes in the thermosyphon. For this purpose, it was decided to measure the pressure difference between the evaporator and condenser, and to design the new facility to maintain a near-constant temperature of the fluid within the thermosyphon thus obtaining the maximum accuracy of the pressure difference measurements which is sensitive to this difference.

2.2. *Experimental results*

A typical experimental run with a mean working fluid temperature of 53.5°C in the thermosyphon is illustrated in Fig. 3(a). This figure shows the behavior of the condenser heat transfer rate Q and pressure difference Δp between the evaporator and condenser as a function of time for different increments and decrements of the heating fluid inlet temperature T_1 and cooling fluid inlet temperature T_2. Thus, for example, region CD corresponds to $T_1 = 59.5$°C and $T_2 = 48$°C, whereas HI to $T_1 = 65$°C and $T_2 = 45$°C. By referring to Fig. 3(a) it is possible to distinguish different regions of the thermosyphon operation: (1) region A–E, which is associated with a regular operation of the thermosyphon with an increase of the cooling load of the condenser; (2) the transition region E–F to thermal blocking; (3) the thermal blocking region F–M; and (4) the transition region M–N to the thermal unblocking or resumption of the regular operation of the thermosyphon.

The cooling load oscillations in Fig. 3(a) in region A–E are due to the heating and cooling fluid inlet temperature variations. These are observed to be of the order of ± 0.2°C, and result from the on–off controller action in the heating and cooling water reservoirs (Fig. 1). The pressure difference oscillations in this region are, however, due not only to the cooling and heating load variations resulting from the thermostatic control systems, but also due to the progressive increase of the wave activity at the liquid film–vapor core interface in the adiabatic

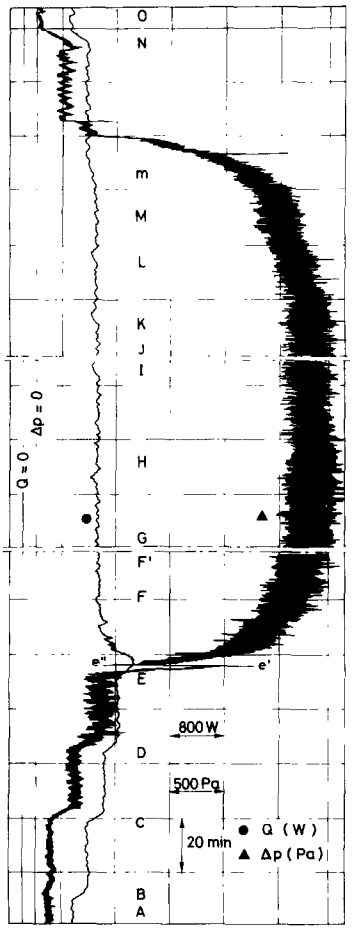

REGION	T_1 (C)	T_2 (C)
A B	58	50.5
B C	58.5	49
C D	59.5	48
D E	60	46.5
E F	60.5	45
F F'	60.5	45
G H	63	45
H I	65	45
J K	62	47
K L	61	48
L M	59.5	48.5
M N	57.5	48.5
N O	56.5	49.5

FIG. 3(a). Timewise distribution of the condenser heat transfer rate and pressure difference between the evaporator and condenser for the mean working fluid temperature of 53.5°C.

region of the thermosyphon as the heat load is increased towards the flooding heat transfer limit. The difference of the working fluid temperatures in the evaporator and condenser is represented in Fig. 3(b), where it is shown that in this region it was hardly detectable by the instruments.

The transition region E–F in Fig. 3(a), or amplified in Fig. 3(b), is associated with an increase of the pressure difference and oscillation of this difference: the heat transfer rate increases up to a maximum and thereafter decreases to a lower value corresponding to that at point E. The very small temperature difference between the fluid in the evaporator and condenser in region e′–e″ (Fig. 3(b)) has an associated large pressure difference drop and a maximum heat transfer rate. In region e″–f this temperature difference becomes negative and of the order of -2°C, whereas at point f it is again reduced to zero and it stabilizes at about 1°C in the thermally blocked region beyond point F. The maximum heat transfer rate and pressure difference peak at point e′ was observed to depend on the degree of sensitivity of the cooling load increase prior to and at point E. When this increase was gradual it was possible to maintain the heat transfer rate close to the maximum achievable in the thermo-

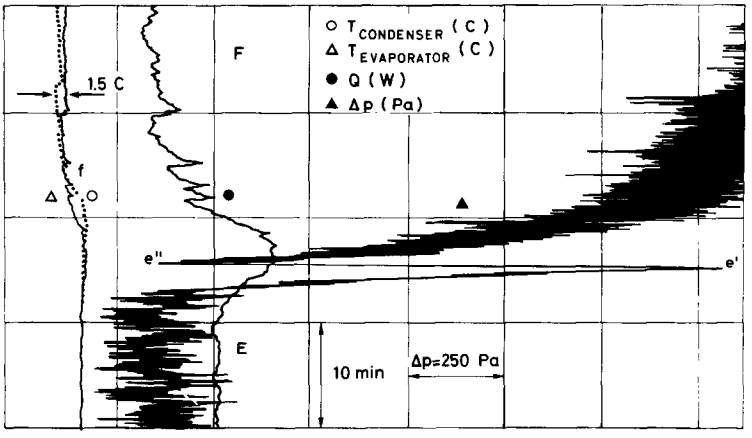

FIG. 3(b). Enlarged detail of the transient from Fig. 3(a).

syphon, with pressure difference oscillations reaching the peak values at e′ and periods depending on the sensitivity of the on–off temperature control of the cooling and heating water reservoirs. The pressure difference peak at point e′ was also observed to depend on the liquid filling in the thermosyphon and its magnitude decreases with the reduction of the filling charge [12]. The pressure decrease from e′ to e″ lasts of the order of 0.5 min.

An increase of the heating fluid temperature T_1 at point F in Fig. 3(a) does not produce a change of the heat transfer carrying capacity of the fluid in the thermosyphon, nor a change in the pressure difference and oscillations. The heat transfer limit in this region may, therefore, be called the *thermal blocking heat transfer limit*. This heat transfer limit was observed for a wide range of $T_1 - T_2$ and up to 60°C (with the maximum achievable as dictated by the design of the experimental apparatus). During the thermal blocking condition the temperatures T_1 and T_2 affected only the average working fluid temperature T^* computed on the basis of the evaporator and condenser temperature measurements (Fig. 2) and not the level of the thermal blocking heat transfer limit. Moreover, by keeping T_2 constant during the thermal blocking condition and only increasing T_1 did not produce a change in the average fluid temperature T^*. An increase (decrease) of T_2 produced an increase (decrease) of T^*. At a certain low value of $T_1 - T_2$ (in Fig. 3(a) this point is approximated by point M with $T_1 - T_2 = 9$°C), the thermosyphon operation reverts to the thermally unblocked state where beyond point m in Fig. 3(a) the temperature difference of the fluid between the evaporator and condenser is hardly noticeable. The attainment of the regular thermosyphon operation upon the reduction of the heat transfer at point M is associated with the decrease of the pressure difference oscillations.

The different states of the heat transfer rates as a function of $T_1 - T_2$ in Fig. 3(a) may be represented more succinctly as shown in Fig. 4. The heat transfer rate corresponding to the onset of the thermally unblocked condition is close to the thermally blocked heat transfer limit (in Fig. 4 close to point LM) and a further decrease of $T_1 - T_2$ reproduces the thermohydrodynamic conditions of the regular thermosyphon operation as illustrated in Fig. 4. The increasing and decreasing temperature difference $T_1 - T_2$ in this figure produces, therefore, a hysteresis effect in the operation of the experimental thermosyphon.

The thermal blocking condition of the experimental thermosyphon of Fig. 2 may also be achieved by operating at a non-constant average temperature T^* of the working fluid as illustrated in Fig. 5. This figure shows the variation of the condenser heat transfer rate Q and average working fluid temperature T^* with the inlet cooling water temperature T_2 for a fixed value of the inlet heating fluid temperature T_1. With T_1 kept constant at 65°C, the thermal blocking heat transfer limit is achieved with the decrease of the cooling water temperature T_2 and can be maintained for varying levels of the average working fluid temperature T^*. In addition, during the variation of this average temperature the difference between the working fluid

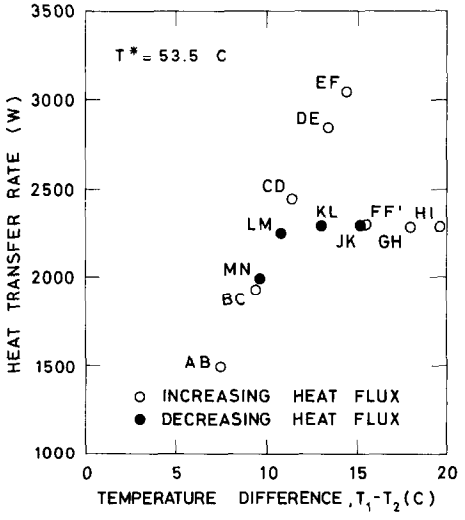

FIG. 4. Representation of the cooling heat transfer rate with the heating and cooling fluid temperature differences for the average working fluid temperature of 53.5°C.

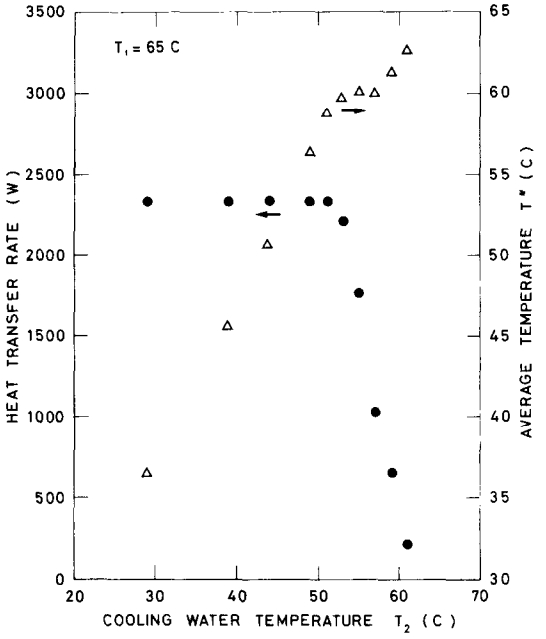

FIG. 5. Representation of the heat transfer rate and average working fluid temperature with the cooling fluid inlet temperature for a constant heating fluid inlet temperature of 65°C.

temperatures in the evaporator and the condenser was never observed to be greater than 2°C.

2.3. *Interpretation of the experimental results*

The purpose of this section is to present a possible interpretation of the experimental data as presented in the previous section. As noted before, the increasing level of pressure oscillations in region A–E of Fig. 3(a) may be associated with an increasing rate of the wave activity on the liquid film–vapor core interface in the adiabatic region of the thermosyphon and an increasing level of the liquid entrainment from the film into the vapor core. Experiments [13] with a thermosyphon similar to that of Fig. 2, but with an imposed heating load in the evaporator and with a transparent adiabatic section, demonstrate that the onset of flooding triggers a large pressure difference between the evaporator and condenser and that the flooding is initiated at the tube entrance in the adiabatic region with a subsequent propagation of disturbances along the entire adiabatic section. The pressure difference from E to e′ in Fig. 3(b) may be, therefore, associated with an instability of the liquid film and the onset of partial film flow reversal. If the heat transfer rate to the evaporator were a controllable parameter, the liquid in the evaporator would be eventually depleted and the thermosyphon would exhibit the oscillation limiting behavior or one of the poorly understood flow regime changes as reported in refs. [10, 11].

In our experimental apparatus the heat flux is not controllable and the complete film flow reversal and liquid depletion from the evaporator may not be possible. As the upward vapor mass flow rate in the adiabatic section of the thermosyphon exceeds the downward liquid mass flow rate in region E–e′ of Fig. 3(b), the wave activity and entrainment processes begin to invade the entire adiabatic section with a consequential rise of pressure between the evaporator and condenser. From e′ to e″ the wave activity and entrainment tend to be progressively transformed towards the exit of the adiabatic section, with a consequential pressure difference decrease as the two-phase flow activities in the tube are reduced. With the condenser temperature remaining constant and the evaporator pressure decreasing from e′ to e″, the heat transfer rate increases as observed in experiments.

From the experimental observations, it was noted before that the evaporator temperature is below the condenser temperature in region e″–f (Fig. 3(b)). The possible causes of this behavior may be attributed to the non-equilibrium effects, i.e. to one or more of the following conditions: (1) the supersaturation of vapor in the evaporator; (2) the subcooling of liquid above the adiabatic section of the condenser; (3) to the thermal capacity effect of the apparatus during the transient operation from E to F in Fig. 3(a). Although during the transient period from E to F the heating and cooling heat transfer rates may not be identical, it appears that beyond point e″ there is a progressive dryout of the evaporator. This is caused by more and more liquid being transferred into the condenser until a new flooding state is achieved at point F corresponding to the thermally blocked condition of the thermosyphon. This new flooding state is most probably located close to or at the adiabatic section exit where the vapor must channel through the liquid above this region. Moreover, to maintain a considerable amount of liquid in the condenser this new flooding state should be the cause of a larger mean pressure difference between the evaporator and condenser, and of more intensive pressure difference oscillations as confirmed by experiments. At point F the equilibrium conditions in the thermosyphon are re-established, as evidenced by a positive temperature difference between the evaporator and condenser (Fig. 3(b)).

The relative constancy of the thermally blocked heat transfer rate beyond point F in Fig. 3(a), as the heating water temperature T_1 is increased with T_2 kept constant, can also be associated with an evaporator operating in a dryout state without the liquid pool. As opposed to the non-equilibrium conditions leading to the thermal blocking heat transfer limit and a new flooding state at point F, the exit from the thermally blocked condition, from point M, is accomplished through a sequence of states close to equilibrium as may be justified by the absence of the temperature difference inversion and significant pressure oscillations (Fig. 3(b)). In summary, therefore, region E–F in Fig. 3(a) may be associated with the transfer of liquid (through a sequence of the non-equilibrium states) from the evaporator to the condenser, where the thermal blocking heat transfer rate corresponds to a new flooding state and a dryout condition in the evaporator.

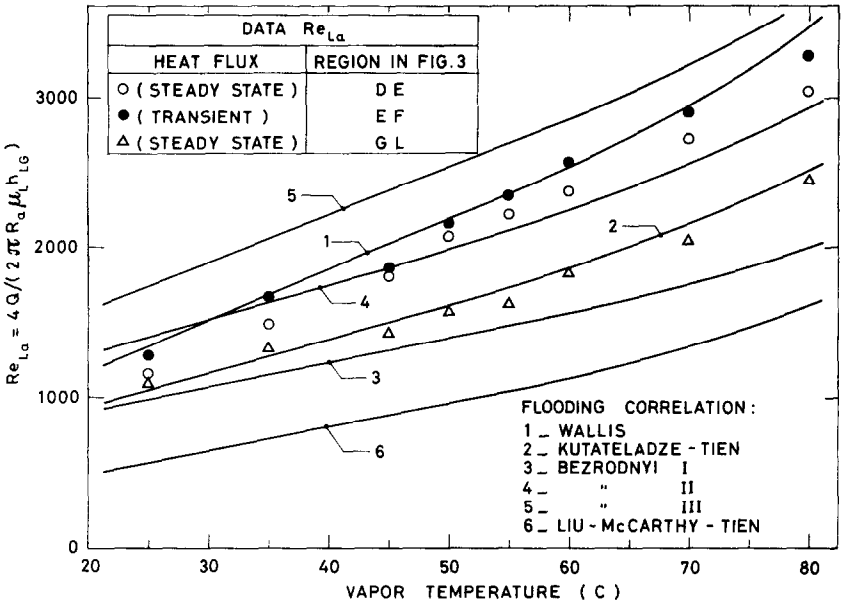

FIG. 6. Relationship between the experimental data and predictions using different flooding correlations.

A decrease of $T_1 - T_2$ below the value corresponding to the thermally blocked heat transfer limit reverts to the regular operation of the thermosyphon corresponding to the same temperature difference between the evaporator and condenser as in region B–C shown in Fig. 3(a). The temperature difference $T_1 - T_2$ drives, therefore, the thermohydrodynamic conditions between the thermally blocked state and the regular operation of the thermosyphon. The hysteresis effect in the heat transfer–temperature difference plot in Fig. 4 is a result, therefore, of different thermohydrodynamic conditions which produce the thermally blocked and unblocked states.

The heat transfer limits corresponding to the transient condition with a maximum heat transfer rate in region E–F, and to the steady state heat transfer limits corresponding to region D–E and to the thermally blocked condition beyond point F as shown in Fig. 3(a) are illustrated in Fig. 6. This figure illustrates a plot of these heat transfer rates expressed in terms of the Reynolds number Re_{La} vs the average working fluid temperature T^* in the thermosyphon. Shown also in this figure are the predictions from the flooding correlations of Wallis [15], Kutateladze–Tien [16], Bezrodnyi [6] and Liu *et al.* [14]. The latter correlation pertains to the onset of flooding in short vertical channels with the liquid pool above.

As shown in Fig. 6, the existing flooding correlations embrace all the experimental data points pertaining to the different thermohydrodynamic conditions of the experimental thermosyphon. Clearly, this implies that the flooding correlations are not very useful to predict different operating conditions of the thermosyphon, and our objective in the next section will be to present an analytical model whereby these conditions may be modeled in a more physical and precise manner.

3. DESCRIPTION OF AN ANALYTICAL MODEL OF THE THERMOSYPHON

The detailed analytical modeling of the thermosyphon illustrated in Fig. 2 is difficult due to the complexity of its geometry and thermohydrodynamic processes occurring within the device. To construct a simple analytical model, use will be made instead of the thermosyphon geometry shown in Fig. 7. This thermosyphon consists of length l, internal tube diameters $D_a = 2R_a$ in the adiabatic and evaporator sections, and $D_c = 2R_c$ in the condenser section. The lengths of the condenser and adiabatic sections are denoted by $\tilde{z}_c$ and $\tilde{z}_a$, respectively.

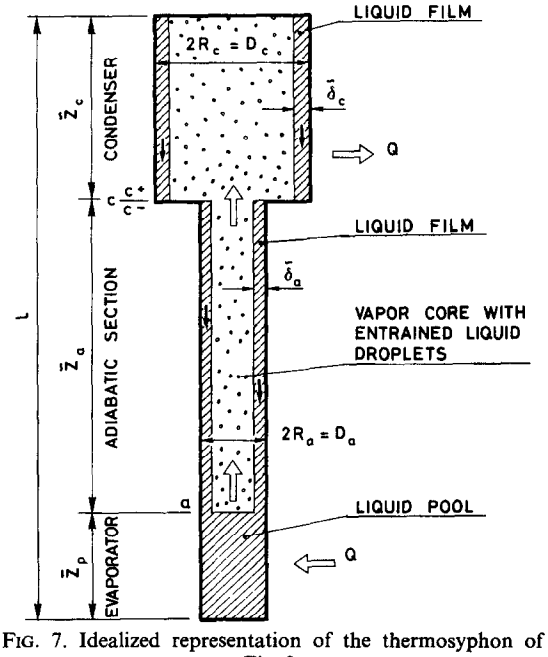

FIG. 7. Idealized representation of the thermosyphon of Fig. 2.

Due to the heat addition in the evaporator, the liquid evaporates from the liquid pool and film regions; the vapor then rises along the central core region of the pipe and is condensed on the wall in the condenser and drained by gravity along the pipe surface into the liquid pool. Due to the evaporation and condensation processes occurring within the thermosyphon, the liquid film thickness in the condenser and adiabatic regions is not uniform or smooth, but usually covered by a complex system of waves which are sheared off by the countercurrently flowing vapor giving rise to the liquid droplet entrainment in the central core region of the thermosyphon. For the purpose of constructing a simple model of these complicated flow phenomena, it will be assumed, however, that the films in the condenser and adiabatic regions can be modeled by average film thicknesses $\tilde{\delta}_c$ and $\tilde{\delta}_a$, respectively, as illustrated in Fig. 7, and that the condenser and adiabatic core regions can be represented by the average values of entrainments E_c and E_a, respectively. The liquid in the films of the condenser and adiabatic sections will be assumed to be at the average temperatures $\tilde{T}_{Lc}$ and $\tilde{T}_{La}$, respectively; that in the liquid pool at an average temperature $\tilde{T}_{Lp}$. The liquid temperatures at sections c and a (Fig. 7) are denoted by T_{Lc} and T_{La}. The films will be assumed to be thin, $\tilde{\delta}/R \ll 1$, the properties of liquid and vapor constant, and the thermosyphon operation away from the thermodynamic critical point, $\rho_G/\rho_L \ll 1$.

3.1. *Lumped parameter analysis*

The analytical modeling of the thermosyphon of Fig. 7 will be accomplished by a lumped parameter analysis first proposed in ref. [17]. The following analysis will, however, include the additional complexities of different tube diameters of the condenser and adiabatic regions, as well as the presence of liquid entrainment in the vapor cores of condenser and adiabatic sections. For the purpose of this paper, the modeling equations given below pertain only to the steady state and not to the more general form that can be used for the transient analysis of the thermosyphon [18].

Denoting by $\Gamma_{c\tilde{z}_c}$ the mass flow rate of vapor condensation per unit tube periphery onto the liquid film in the condenser, by $\Gamma_{c\tilde{z}_a}$ the mass flow rate of vapor condensation per unit tube periphery onto the liquid film in the adiabatic region, by Γ_{Lc} the mass flow rate of liquid per unit tube periphery flowing at $\tilde{z}_c$ into the adiabatic region, by Γ_{La} the mass flow rate of liquid per unit tube periphery flowing at $\tilde{z}_a$ into the liquid pool, by M_c the mass flow rate of vapor and liquid droplets per unit area (πR_c^2) at section c, and by M_a the mass flow rate of vapor and liquid droplets per unit area (πR_a^2) in the adiabatic section at a, it may be shown from the control volume mass and energy balance equations on the liquid films, liquid pool and vapor–droplet cores that

$$\Gamma_{c\tilde{z}_c} = \Gamma_{Lc^+}, \quad \Gamma_{c\tilde{z}_a} = \Gamma_{La} - \Gamma_{Lc^-}, \quad \Gamma_{Lc^-} = \Gamma_{Lc^+}\frac{R_c}{R_a} \tag{1}$$

$$M_a = \frac{2}{R_a}\Gamma_{La}, \quad M_{c^+} = \frac{2}{R_c}\Gamma_{c\tilde{z}_c}, \quad M_{c^-} = \left(\frac{R_c}{R_a}\right)^2 M_{c^+} \tag{2}$$

$$M_a - M_{c^-} = \frac{2}{R_a}\Gamma_{c\tilde{z}_a} \tag{3}$$

$$M = \pi R_a^2 \rho_L \left\{ l - \tilde{z}_a\left(1 - \frac{\tilde{\delta}_a}{R_a}\right)^2\left(1 - \frac{\rho_{ha}}{\rho_L}\right) - \tilde{z}_c\left[1 - \left(\frac{R_c}{R_a}\right)^2 + \left(\frac{R_c}{R_a}\right)^2\left(1 - \frac{\tilde{\delta}_c}{R_c}\right)^2\left(1 - \frac{\rho_{hc}}{\rho_L}\right)\right]\right\} \tag{4}$$

$$\Gamma_{L\tilde{z}_c}[x_c h_{LGc} - C_L(\tilde{T}_{Lc} - T_{csat})] - \Gamma_{Lc^+} C_L(T_{Lc} - \tilde{T}_{Lc}) + q_{wc}\tilde{z}_c = 0 \tag{5}$$

$$\Gamma_{c\tilde{z}_a}[x_a h_{LGa} - C_L(\tilde{T}_{La} - T_{asat})] - \Gamma_{La} C_L(T_{La} - \tilde{T}_{La}) + \Gamma_{Lc^-} C_L[(T_{Lc} - T_{La}) + (T_{La} - \tilde{T}_{La})] = 0 \tag{6}$$

$$-M_a[x_a h_{LGa} - C_L(\tilde{T}_{Lp} - T_{asat})] + \frac{2}{R_a}\Gamma_{La} C_L(T_{La} - \tilde{T}_{Lp}) + \frac{2}{R_a} q_{wp}\tilde{z}_p = 0 \tag{7}$$

$$M_a h_{ha} = \frac{R_c}{R_a^2} 2\Gamma_{c\tilde{z}_c}\tilde{h}_{hc} + \frac{2}{R_a}\Gamma_{c\tilde{z}_a}\tilde{h}_{ha} \tag{8}$$

where M is the total mass of the working fluid in the thermosyphon and where the derivation of equation (8) for the energy balance of the vapor and liquid in the core assumes a saturation condition at a single average pressure. Similarly, the control volume momentum balances give

$$-U_{G\tilde{z}_c}\Gamma_{c\tilde{z}_c} + B_{Lc^+}\frac{\Gamma_{Lc^+}^2}{\rho_L \tilde{\delta}_c} = \tilde{\delta}_c[\rho_L g\tilde{z}_c - (p_c - p_t)] - \tilde{z}_c(\tau_{wc} + \tau_{ic}) \tag{9}$$

$$-U_{G\tilde{z}_a}\Gamma_{c\tilde{z}_a} + B_{La}\frac{\Gamma_{La}^2}{\rho_L \tilde{\delta}_a} - B_{Lc^-}\frac{\Gamma_{Lc^-}^2}{\rho_L \tilde{\delta}_c} = \tilde{\delta}_a[\rho_L g\tilde{z}_a - (p_a - p_c)] - \tilde{z}_a(\tau_{wa} + \tau_{ic}) \tag{10}$$

$$U_{G\tilde{z}_c}\Gamma_{c\tilde{z}_c}\frac{2}{R_c} + B_{Gc^+}\frac{M_{c^+}^2}{\rho_{hc}} = g\rho_{hc}\tilde{z}_c - (p_c - p_t) + \frac{2}{R_c}\tilde{z}_c\tau_{ic} \tag{11}$$

$$U_{G\tilde{z}_a}\Gamma_{c\tilde{z}_a}\frac{2}{R_a} + B_{Ga}\frac{M_a^2}{\rho_{ha}} - B_{Gc^-}\frac{M_c^2}{\rho_{hc}} = g\rho_{ha}\tilde{z}_a - (p_a - p_c) + \frac{2}{R_a}\tilde{z}_a\tau_{ia} \tag{12}$$

where the homogeneous core densities ρ_{hc} and ρ_{ha}, qualities x_c and x_a, and void fractions α_c and α_a can be expressed in terms of the liquid droplet entrainments E_c and E_a, i.e.

$$\rho_{hc} = \alpha_c\rho_G + (1 - \alpha_c)\rho_L \tag{13}$$

$$\rho_{ha} = \alpha_a\rho_G + (1 - \alpha_a)\rho_L \tag{14}$$

$$x_c = 1 - \frac{E_c}{1-E_c}\frac{2}{R_c}\frac{\Gamma_{Lc^+}}{M_{c^+}} \tag{15}$$

$$x_a = 1 - \frac{E_a}{1-E_a}\frac{2}{R_a}\frac{\Gamma_{La}}{M_a} \tag{16}$$

$$\alpha_c = \left(1 + \frac{1-x_c}{x_c}\frac{\rho_G}{\rho_L}\right)^{-1} \tag{17}$$

$$\alpha_a = \left(1 + \frac{1-x_a}{x_a}\frac{\rho_G}{\rho_L}\right)^{-1}. \tag{18}$$

The coefficients B_{Lc^+}, B_{Lc^-}, B_{La}, B_{Gc^+}, B_{Gc^-} and B_{Ga} in equations (9)–(12) represent the effect of the deviation of the velocity profiles of liquid and vapor at sections c^+, c^- and a from the uniform profiles. Thus, for example

$$B_{Lc^+} = \frac{2\pi R_c \tilde{\delta}_c\left(1 - \dfrac{\tilde{\delta}_c}{2R_c}\right)\rho_L}{(2\pi R_c)^2\Gamma_{Lc}^2}\int_{R_c-\tilde{\delta}_c}^{R_c} 2\pi r\rho_L U_L^2\,dr \tag{19}$$

where U_L is the local axial liquid velocity.

In the steady state the heat transfer supplied to the evaporator and removed in the condenser must balance, i.e.

$$Q = -2\pi R_c \tilde{z}_c q_{wc} = 2\pi R_a \tilde{z}_p q_{wp}. \tag{20}$$

Using this relation, setting $U_{G\tilde{z}_c} = U_{ic}$ and $U_{G\tilde{z}_a} = U_{ia}$, and manipulating the foregoing equations yields a set of 15 equations with 42 variables. By specifying the 26 variables R_c, R_a, h_{LGc}, h_{LGa}, $C_L(T_{Lc}-T_{csat})$, $C_L(T_{La}-T_{asat})$, $C_L(T_{Lc}-T_{asat})$, U_{ic}, ρ_L, ρ_G, g, τ_{wc}, τ_{ic}, U_{ia}, τ_{wa}, τ_{ia}, B_{Lc^+}, B_{La}, B_{Lc^-}, B_{Gc^+}, B_{Ga}, B_{Gc^-}, E_a, E_c, M and l it is then possible to combine the remaining 16 variables for the solution of $Q = Q(\tilde{\delta}_c)$ or $Q = Q(\tilde{\delta}_a)$. Among the 26 variables above the shear stresses τ_{wc}, τ_{wa}, τ_{ic} and τ_{ia}, and the interface velocities U_{ic} and U_{ia} may be specified as in ref. [17] with coefficients u_1 and u_2 in the interfacial shear stresses given by

$$u_{1c} = 0.2754\times 10^{9.07/(N_{Lc}Ca_c^{1/2})}$$
$$u_{1a} = 0.2754\times 10^{9.07/(N_{La}Ca_a^{1/2})} \tag{21}$$

$$u_{2c} = 1.63 + \frac{4.74}{N_{Lc}Ca_c^{1/2}}, \quad u_{2a} = 1.63 + \frac{4.74}{N_{La}Ca_a^{1/2}} \tag{22}$$

$$N_{Lc} = \left[\frac{gD_c^3\rho_L^2}{\mu_L^2}\right]^{1/2}$$

$$N_{La} = \left[\frac{gD_a^3\rho_L^2}{\mu_L^2}\right]^{1/2} = N_{Lc}\left(\frac{R_a}{R_c}\right)^{3/2} \tag{23}$$

$$Ca_c = \frac{\mu_L^2}{\sigma\rho_L D_c}, \quad Ca_a = \frac{\mu_L^2}{\sigma\rho_L D_a} = Ca_c\left(\frac{R_c}{R_a}\right). \tag{24}$$

The subcoolings of the liquid films may be accounted for in the model by assuming that the film temperature distribution follows Nusselt's laminar flow solution of condensation on a vertical surface. Hence

$$\frac{C_L(T_{csat}-T_{Lc})}{h_{LGc}} = \frac{C_L(\Delta T)_c}{h_{LGc}} \approx \frac{C_L}{h_{LGc}}\left(\frac{Q}{2\pi R_c 0.943\tilde{z}_c}\right)^{4/3}\left(\frac{\mu_L\tilde{z}_c}{g\rho_L^2 h_{LGc}k_L^3}\right)^{1/3} \tag{25}$$

$$\frac{C_L(T_{asat}-T_{La})}{h_{LGa}} = \frac{C_L(\Delta T)_a}{h_{LGa}} \approx \frac{C_L}{h_{LGa}}\left(\frac{Q}{2\pi R_a 0.943\tilde{z}_a}\right)^{4/3}\left(\frac{\mu_L\tilde{z}_a}{g\rho_L^2 h_{LGa}k_L^3}\right)^{1/3}. \tag{26}$$

By eliminating (p_c-p_i) between equations (9) and (11), (p_a-p_c) between equations (10) and (12), assuming that $h_{LGa}\approx h_{LGc} = h_{LG}$, ignoring the subcooling of liquid in the adiabatic region $(T_{asat}-T_{La}=0)$, and performing the non-dimensionalization according to

$$Q^* = \frac{Q}{8\mu_L R_c h_{LG}} \tag{27}$$

$$\mu^* = \frac{\mu_G}{\mu_L}, \quad \rho^* = \frac{\rho_G}{\rho_L} \tag{28}$$

$$E = \frac{1-2E_a}{1-2E_c}\frac{1-E_c}{1-E_a} \tag{29}$$

$$l^* = \frac{l}{R_a}, \quad h^* = \frac{M}{\rho_L\pi R_a^3} = \frac{Q_L}{\pi R_a^3} \tag{30}$$

$$x_{1c}^* = \frac{\tilde{z}_c}{R_c}, \quad x_{1a}^* = \frac{\tilde{z}_a}{R_a} \tag{31}$$

$$x_{2c}^* = \frac{\tilde{\delta}_c\tilde{z}_c}{R_c^2}, \quad x_{2a}^* = \frac{\tilde{\delta}_a\tilde{z}_a}{R_a^2} \tag{32}$$

the modeling equations may be transformed into the following forms:

$$\left(\frac{Q^*}{x_c + C_L(\Delta T)_c/h_{LG}}\right)^2\frac{1}{2\pi}\left\{(1-B_{Lc^+}) - 2\left(\frac{x_{2c}^*}{x_{1c}^*}\right)\left[1-2\left(\frac{x_{2c}^*}{x_{1c}^*}\right)\frac{\rho_L}{\rho_{hc}}B_{GC^+}\right]\right\} - \left(\frac{Q^*}{x_c + C_L(\Delta T)_c/h_{LG}}\right)\left[\left(\frac{f_w}{f_{wl}}\right)_c\frac{A_{wc}}{4}x_{1c}^*\frac{x_{1c}^*}{x_{2c}^*} + \left(\frac{f_i}{f_{il}}\right)_c\frac{A_{ic}}{2}\mu^* x_{1c}^*\left(1+2\frac{\rho_L}{\rho_{hc}}\frac{x_{2c}^*}{x_{1c}^*}\right)\left(1+2\frac{x_{2c}^*}{x_{1c}^*}\right)\right] + N_{Lc}^2\frac{\pi}{256}x_{1c}^*\left(\frac{x_{2c}^*}{x_{1c}^*}\right)^2\left(1-\frac{\rho_{hc}}{\rho_L}\right) = 0 \tag{33}$$

$$\left(\frac{Q^*}{x_c + C_L(\Delta T)_c/h_{LG}}\right)^2\frac{1}{2\pi}\left\{1-E-B_{La} - 2\left(\frac{x_{2a}^*}{x_{1a}^*}\right)\left[1-E-2\left(\frac{x_{2a}^*}{x_{1a}^*}\right)\frac{\rho_L}{\rho_{ha}}B_{Ga}\right.\right.$$

$$-E^2B_{Lc^-}\frac{R_a}{2R_c}\frac{x^*_{1c}}{x^*_{2c}}+E^2\frac{\rho_L}{\rho_{hc}}B_{Gc^-}2\left(\frac{x^*_{2a}}{x^*_{1a}}\right)\Bigg]\Bigg\}-\frac{R_aE}{R_c}$$
$$\times\left(\frac{Q^*}{x_c+C_L(\Delta T)_c/h_{LG}}\right)\Bigg[\left(\frac{f_w}{f_{wl}}\right)_a\frac{A_{wa}}{4}x^*_{1a}\left(\frac{x^*_{1a}}{x^*_{2a}}\right)$$
$$+\left(\frac{f_i}{f_{il}}\right)_a\frac{A_{ia}}{2}\mu^*x^*_{1a}\left(1+2\frac{\rho_L}{\rho_{ha}}\frac{x^*_{2a}}{x^*_{1a}}\right)\left(1+2\frac{x^*_{2a}}{x^*_{1a}}\right)\Bigg]$$
$$+N^2_{Lc}\frac{\pi}{256}x^*_{1a}\left(\frac{x^*_{2a}}{x^*_{1a}}\right)\left(\frac{R_a}{R_c}\right)^3\left(\frac{R_aE}{R_c}\right)^2\left(1-\frac{\rho_{ha}}{\rho_L}\right)=0 \tag{34}$$

$$x^*_{1a}=\frac{l^*}{\left(1-\frac{\rho_{ha}}{\rho_L}\right)\left(1-\frac{x^*_{2a}}{x^*_{1a}}\right)^2}\Bigg[1-\frac{h^*}{l^*}-\left(\frac{R_c}{R_a}\right)\frac{x^*_{1c}}{l^*}$$
$$+\left\{1-\left(\frac{R_c}{R_a}\right)^2\left[1-\left(1-\frac{x^*_{2c}}{x^*_{1c}}\right)^2\left(1-\frac{\rho_{hc}}{\rho_L}\right)\right]\right\}\Bigg] \tag{35}$$

$$\left(\frac{f_w}{f_{wl}}\right)_c=\frac{0.079}{16}\left[\frac{16}{\pi}\frac{Q^*}{x_c+C_L(\Delta T)_ch_{LG}}\right]^{0.75}$$
$$\text{if}\quad\frac{16Q^*}{\pi(x_c+C_L(\Delta T)_ch_{LG})}\geqslant 1000$$
$$=1\quad\text{otherwise} \tag{36}$$

$$\left(\frac{f_w}{f_{wl}}\right)_a=\frac{0.079}{16}\left[\frac{16}{\pi}\frac{Q^*}{x_c+C_L(\Delta T)_ch_{LG}}\frac{R_c}{R_aE}\right]^{0.75}$$
$$\text{if}\quad\frac{16Q^*}{\pi(x_c+C_L(\Delta T)_ch_{LG})}\frac{R_c}{R_aE}\geqslant 1000$$
$$=1\quad\text{otherwise} \tag{37}$$

$$\left(\frac{f_i}{f_{il}}\right)_c=\frac{Q^*}{2\pi\mu^*}\frac{\left(2+\frac{\rho_{hc}}{\rho_L}\frac{x^*_{1c}}{x^*_{2c}}\right)}{(x_c+C_L(\Delta T)_c/h_{LG})}$$
$$\times\left[0.005+u_{1c}\left(\tfrac{1}{2}N_{Lc}Ca_c^{1/2}\frac{x^*_{2c}}{x^*_{1c}}\right)^{u_{2c}}\right] \tag{38}$$

$$\frac{C_L(\Delta T)_c}{h_{LG}}=\frac{1}{x^*_{1c}}\frac{Pr_L}{N^{2/3}_{Lc}}Q^{*4/3}\left(\frac{8}{0.943\pi}\right)^{4/3}. \tag{40}$$

Substituting equations (13)–(18) and (35)–(40) into (33) and (34) gives

$$f_1\left(Q^*,\frac{x^*_{2c}}{x^*_{1c}},\text{Parameters}\right)=0 \tag{41}$$

$$f_2\left(Q^*,\frac{x^*_{2a}}{x^*_{1a}},\frac{x^*_{2c}}{x^*_{1c}},\text{Parameters}\right)=0 \tag{42}$$

from which we may solve for

$$Q^*=Q^*\left(\frac{x^*_{2a}}{x^*_{1a}},\text{Parameters}\right)=0 \tag{43}$$

where the independent parameters of this solution are as follows:

$$\text{Parameters}=\{E_a, E_c, N_{Lc}, Ca_c, l^*, h^*/l^*, x^*_{1c}, Pr_L, \rho^*, \mu^*, R_a/R_c, A_{wa}, A_{ia}, B_{Lc^+}, B_{Gc^+}, A_{wc}, A_{ic}, B_{La}, B_{Ga}, B_{Lc^-}, B_{Gc^-}\}. \tag{44}$$

The velocity profile coefficients may be set equal to unity in view of other more critical assumptions in the analysis reducing equation (44) into the following form:

$$\text{Parameters}=\{E_a, E_c, N_{Lc}, Ca_c, l^*, h^*/l^*, x^*_{1c}, Pr_L, \rho^*, \mu^*, R_a/R_c\}. \tag{45}$$

The entrainment parameters E_a and E_c are, clearly, not independent of the thermohydrodynamic processes in the thermosyphon (see, e.g. ref. [19]), but in the model they will be treated as such. The parameter N_{Lc} is the ratio of gravity to viscous forces and may be called the two-phase Grashof number, whereas Ca_c is the capillary number and represents a ratio of the viscous to the surface tension forces. The parameter h^*/l^* represents the effect of the liquid filling in the thermosyphon, and if it is sufficiently small the thermosyphon may become dry under the imposed thermal loading producing the dryout heat transfer limit [17]. To determine this limiting operation of the thermosyphon it may be noted from Fig. 7 that

$$(x^*_{1a})_{max}=\left(\frac{\bar{z}_a}{R_a}\right)_{max}=\frac{l-\bar{z}_c}{R_a}=l^*-\left(\frac{R_c}{R_a}\right)x^*_{1c} \tag{46}$$

which upon substitution into equation (35) yields

$$\left(\frac{x^*_{2a}}{x^*_{1a}}\right)_{\text{no pool}}=1-\left[\frac{1-\frac{h^*}{l^*}-\left(\frac{R_c}{R_a}\right)\frac{x^*_{1c}}{l^*}\left[1-\left(\frac{R_c}{R_a}\right)^2\left\{1-\left(1-\frac{x^*_{2c}}{x^*_{1c}}\right)^2\left(1-\frac{\rho_{hc}}{\rho_L}\right)\right\}\right]}{\left(1-\frac{R_c}{R_a}\frac{x^*_{1c}}{l^*}\right)\left(1-\frac{\rho_{ha}}{\rho_L}\right)}\right]^{1/2}. \tag{47}$$

$$\left(\frac{f_i}{f_{il}}\right)_a=\frac{Q^*}{2\pi\mu^*}\frac{\left(2+\frac{\rho_{ha}}{\rho_L}\frac{x^*_{1a}}{x^*_{2a}}\right)}{(x_c+C_L(\Delta T)_c/h_{LG})}$$
$$\times\left[0.005+u_{1a}\left(\tfrac{1}{2}N_{La}Ca_a^{1/2}\frac{x^*_{2a}}{x^*_{1a}}\right)^{u_{2a}}\right]\left(\frac{R_c}{R_aE}\right) \tag{39}$$

Note from equations (31) and (32) that $x^*_{2a}/x^*_{1a}=\bar{\delta}_a/R_a$ and that a physical solution of equation (43) is possible only if $x^*_{2a}/x^*_{1a}\leqslant(x^*_{2a}/x^*_{1a})_{\text{no pool}}$ or, for large h^*/l^* where the inequality prevails, until $dQ^*/d(x^*_{2a}/x^*_{1a})=0$ at which point the solution for the heat transfer Q^* may be identified with the heat transfer rate to the thermosyphon causing the flooding or countercurrent limiting flow operation [17].

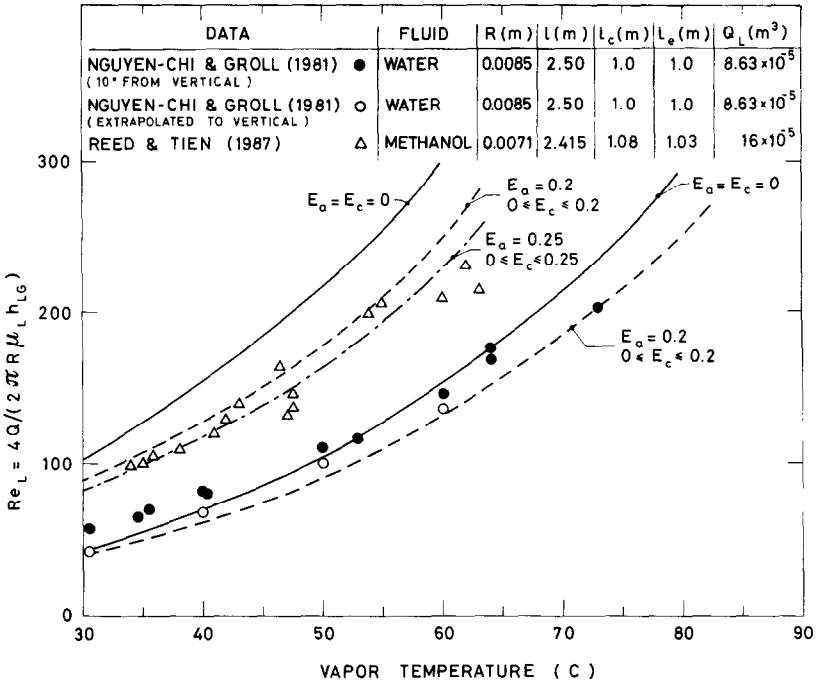

FIG. 8. Relationship between the flooding data with imposed evaporator heat transfer and model predictions with different entrainments.

3.2. *Verification of the analytical model with the existing data from literature*

In this section the thermosyphon model presented above will be verified by using the data from literature with thermosyphons operating with imposed heat transfer in the evaporator. This verification is necessary in view of the many assumptions made in the construction of the model presented above. The thermosyphons used for the verification of the model are of simple designs consisting of vertical tubes closed at both ends where the heat is added to the evaporator sections at the bottom and removed in the condenser sections at the top.

The comparison between the experimental data [9, 20] and model predictions of the flooding heat transfer rates expressed in terms of Re_L for various vapor temperatures is illustrated in Figs. 8 and 9. As shown in Fig. 8, the water data of Nguyen-Chi and Groll [9] can be modeled well with entrainment levels of less than 25%, whereas the methanol data of Reed and Tien [20] are overpredicted up to 40% with a model which assumes no entrainment. With the entrainment of about 25% the latter data are, however, well modeled. Moreover, the model prediction of the flooding heat transfer rates with entrainments in the condenser which are less than those in the adiabatic section do not affect this prediction. The water and methanol data of Prenger in Fig. 9 (as reported in ref. [20]) are very well modeled at the lower vapor temperatures without the entrainment, whereas at higher temperatures the model tends to underpredict the data by less than 30%.

Reed and Tien [20] also presented a model for the single diameter thermosyphon without accounting for entrainment by extending the analysis of ref. [17] to include different film thicknesses in the condenser, adiabatic and evaporator regions. Their comparison of the model predictions with data of Figs. 8 and 9 is very reasonable for the data of Reed and Tien, and at lower temperatures overpredicts the water data of Prenger by about 100% and underpredicts the water data of Nguyen-Chi and Groll by about 25%. The difference in predictions between the present model and that of Reed and Tien may not only be attributed to the slightly different modeling approaches, but also due to the use of different constitutive equations in the analysis.

From the above discussion, it may be concluded that the present model predicts well the available experimental data of flooding in single tube diameter thermosyphons and that the neglect of entrainment in the model may not always be justifiable. As noted previously, however, the entrainment of liquid in the vapor is dependent on the thermohydrodynamic state of the two-phase flow in the thermosyphon; its specification in the model in terms of independent parameters E_c and E_a serves only the purpose of studying its effect on the predicted flooding and dryout heat transfer rates in a relatively simple manner. In the next section, therefore, an attempt will be made to predict the unblocked and blocked limiting heat transfer rates of the experimental thermosyphon shown in Fig. 2 using the model described above.

4. MODELING AND ANALYSIS OF DATA

As noted in Section 2 and shown in Fig. 6, the available flooding correlations are individually not

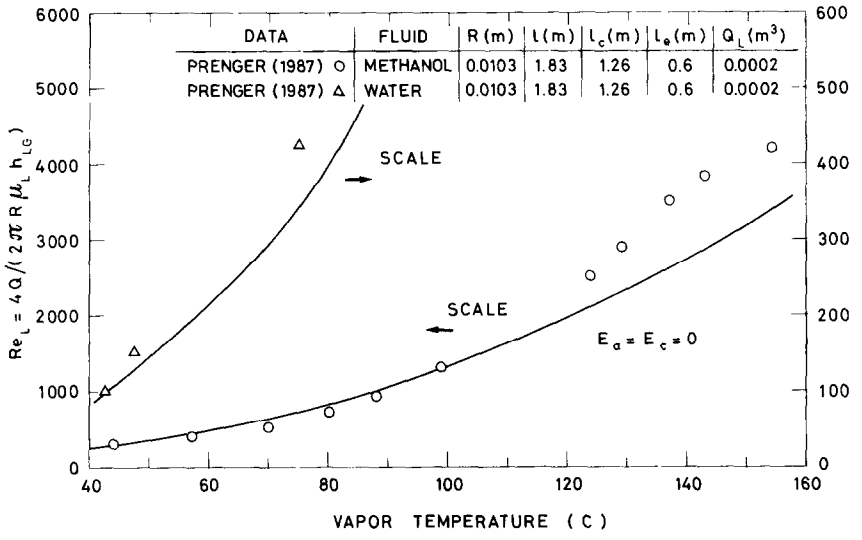

FIG. 9. Relationship between the flooding data with imposed evaporator heat transfer and model predictions with no entrainment.

suitable to predict the different heat transfer limits of the experimental thermosyphon. For this reason, an analytical model was presented in the previous section for the purpose of providing a more suitable means of predicting the thermosyphon performance with the imposed convection boundary conditions. The assumptions in the model, of the near uniformity of pressure, predominance of the saturation condition in the core and smallness of the liquid subcooling in films of the thermosyphon, may be justified in view of the fact that the maximum temperature and pressure difference in experiments were always less than 5°C and 2500 Pa, respectively.

4.1. *Identification of the model thermosyphon geometry*

An application of the model discussed in the previous section requires at first a reduction of the geometry of the experimental thermosyphon illustrated in Fig. 2 to that of the model geometry shown in Fig. 7. Towards this objective it should be noted that the model accounts for the thermohydrodynamic processes within the thermosyphon in an average manner and that the details of the heat transfer processes in the evaporator and condenser are not explicitly modeled, since the model only involves the heat transfer rates in these regions. Although the distribution of heat transfer rates in the evaporator and condenser may not be very important in maintaining the heat transfer limits, they should, nevertheless, be important in determining the stability conditions between different quasi-steady states. The importance of maintaining as closely as possible the hydrodynamic conditions between the two thermosyphons cannot, however, be underestimated. In our view it is necessary to maintain the volumes of the condensers and evaporators of the two thermosyphons identical, since these volumes provide the necessary compressible volumes for the maintenance of the thermally blocked and unblocked states. This approach of maintaining the volumes of the condensers and evaporators identical may be contrasted with a less plausible option which requires that the temperature difference between the heat transfer surface and working fluid is maintained identical.

Table 1. Geometry of the model thermosyphon for use in the analytical model of the experimental thermosyphon

Case	R_a (m)	R_c (m)	$\tilde{z}_{p0}$ (m)	$\tilde{z}_{a0}$ (m)	$\tilde{z}_c$ (m)	l (m)
Volume	0.016	0.103	8.65	3.62	0.51	12.78
ΔT Constant	0.016	0.103	14.44	3.62	1.32	19.38

The geometry of the model thermosyphon in Fig. 7 may, therefore, involve the two limiting situations noted above with the dimensions as given in Table 1 and a filling charge identical to the experimental thermosyphon (0.006 m³). Note in Table 1 that the evaporator and adiabatic section diameters are assumed to be identical to the diameter of the adiabatic region of the experimental thermosyphon (Fig. 2) and that the internal diameters of the condenser sections are maintained identical between the two thermosyphons. The lengths $\tilde{z}_{p0}$ and $\tilde{z}_{a0}$ pertain to the evaporator and adiabatic lengths, respectively, in an unoperating condition of the thermosyphon. For the case where the volumes of the model and experimental thermosyphon are matched (case Volume in Table 1), the procedure for calculating $\tilde{z}_{p0}$ and $\tilde{z}_c$ should be clear. In the case of ΔT Constant, however, it is required that

$$Q/\Delta T = A_{\text{model}} h_{\text{model}} = A_{\text{actual}} h_{\text{actual}} \qquad (48)$$

where A is the heat transfer area and h the heat transfer coefficient. For the condenser, the above equation may be written as follows [21]:

$$2\pi R_c \tilde{z}_c \left(\frac{1}{\tilde{z}_c}\right)^{1/4} = A_{actual} \left(\frac{1}{d_{coil} N_{coil}}\right)^{1/4} \quad (49)$$

where $A_{actual} = 0.53$ m^2, $d_{coil} = 0.01$ m, and $N_{coil} = 20$. For the evaporator, the heat transfer coefficients are difficult to estimate reliably for the nucleate boiling processes in confined spaces of small tube diameters and different tube lengths for either the model or experimental thermosyphon: it will be assumed that they have the same order of magnitude in the two thermosyphons. Equation (48) gives, therefore, that $A_{model} = A_{actual} = 1.45$ m^2 from which follows the dimension of $\tilde{z}_{p0}$ given in Table 1. The transformation of the geometry of the experimental thermosyphon of Fig. 2 to the model geometry of Fig. 7, for either of the two cases of Table 1, produces a considerable geometrical distortion. This implies that the actual temperature distributions in the experimental and model thermosyphons should be quite different, and that the replacement of the experimental thermosyphon by the model thermosyphon may not be justifiable, particularly in the evaporator where there may exist a considerable temperature gradient of the working fluid. Realizing, however, that the model is a lumped parameter model and that it preserves the tube diameters and conservation of mass in the adiabatic regions of the two thermosyphons, the noted geometrical distortions of the evaporator and condenser of the model thermosyphon should not be too important for large liquid fillings where the limiting thermosyphon operation is by flooding.

4.2. *Interpretation of data by the model*

For the case of Volume in Table 1, the relationship between the predicted flooding heat transfer rates, expressed in the form of a Reynolds number Re_{La}, vs the vapor temperature for different values of entrainments in the adiabatic and condenser sections is illustrated in Fig. 10. Shown also in this figure are the experimental data of heat transfer rates expressed in the form of Re_{La} for the three different regions of operation of the experimental thermosyphon as delineated in Fig. 3(a), and the predicted values of the circulating working fluid volumes (the volume of working fluid not in the pool of the evaporator) Q'_L at the flooding conditions. From the results of Fig. 10 it may be concluded that the level of entrainment in the condenser of less than 30% has no effect on the predicted flooding heat transfer rates for all entrainment levels in the adiabatic region of less than 30%. Both the entrainment in the evaporator and in the condenser, have, however, a pronounced effect on the distribution of Q'_L, with the results being limited by the two bands with $(0 \leqslant E_a \leqslant 0.3,\ E_c = 0)$ and $(0 \leqslant E_a \leqslant 0.3,\ E_c = 0.3)$.

By comparing the predicted flooding heat transfer rates or Re_{La} with the experimental data in Fig. 10 it may be possible to establish the entrainment levels in the experimental thermosyphon before the achievement of the thermal blocking conditions. Figure 11 illustrates the results of this matching for the heat transfer rates in region D–E and maximum heat transfer rates in region E–F shown in Fig. 3(a). As discussed in Section 2, the exact values of the heat transfer rates corresponding to the onset of flooding in the experimental thermosyphon are not well defined by the data, but lie somewhere between the two limiting values of heat transfer rates in regions DE and EF. For this reason, the dashed curve in Fig. 11 can be identified as representing an average value of the entrainment in the thermosyphon at the onset of flooding. Corresponding to these average values of entrainment the results for Q'_L in Fig. 10 may then be used to establish the two curves for Q'_L shown in Fig. 11 corresponding to the two possible entrainment levels in the condenser.

The reason for reporting the predicted values of Q'_L will serve the purpose for the interpretation of the thermally blocked heat transfer data by the model. As interpreted in Section 2, the transient period from E to F in Fig. 3(a) which produces the thermally blocked conditions in the thermosyphon is a result of the transfer of liquid from the pool of the evaporator into the condenser and the establishment of a new flooding state in the adiabatic region and the dryout condition in the evaporator. To predict the dryout state of the thermosyphon by the model it should only be necessary to use now the model with a new value of the liquid filling corresponding to Q'_L and determine the corresponding dryout heat transfer rate. The result of this procedure is illustrated in Fig. 12 for different values of entrainments and corresponding to the two limiting values of Q'_L for the case Volume of Table 1. As seen from this figure, the thermally blocked heat transfer rates may be predicted within $\pm 30\%$ for very reasonable values of entrainments in the thermosyphon. Moreover, the actual value of Q'_L should be between $Q'_{L,MIN}$ and $Q'_{L,MAX}$ and the data should be predicted with quite low values of the entrainment. These low values of entrainment during the thermal blocking conditions of the thermosyphon should be expected in view of the low film flow rates and the available experimental data [22] from which the entrainment correlation may be deduced and used as a dependent variable in the model.

The adopted procedure for the prediction of heat transfer rates of the thermally blocked conditions in the thermosyphon for the case of Volume in Table 1 may be repeated for the case of ΔT Constant. Thus Fig. 13 corresponds to Fig. 10 and illustrates the experimental data together with the predicted flooding heat transfer rates and circulating working fluid volumes as a function of the vapor temperature for different values of entrainment. By matching the data with the corresponding entrainment values in this figure, it is then possible to generate the results in Fig. 14 (which is equivalent to Fig. 11) and determine the two possible limits of $Q'_{L,MIN}$ and $Q'_{L,MAX}$. With these values of liquid fillings the model can then be used to establish the dryout heat transfer limits for different

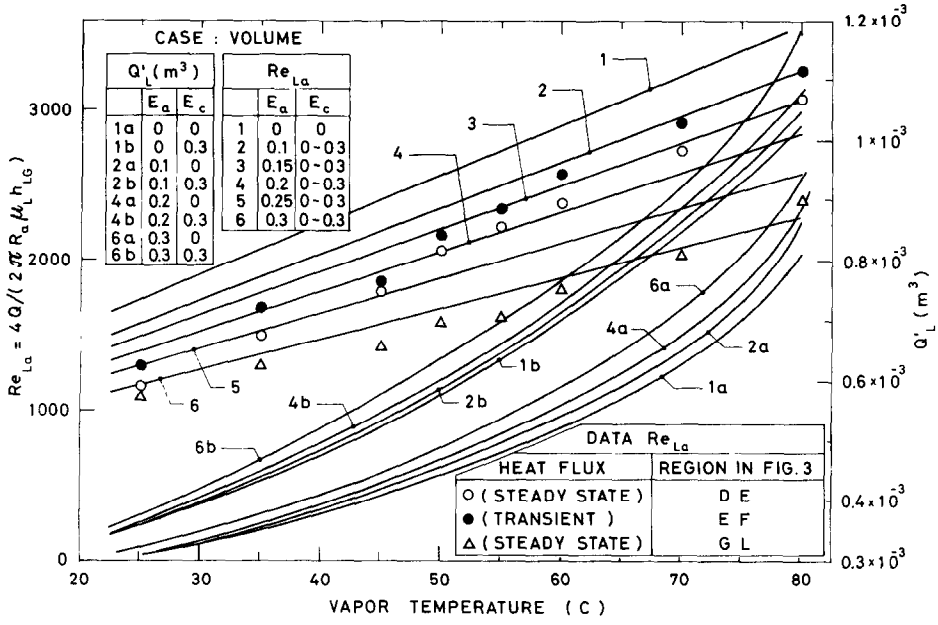

FIG. 10. Relationship between the predicted heat transfer rates and circulating volumes of the working fluid at flooding with the vapor temperature for different entrainments for the case Volume.

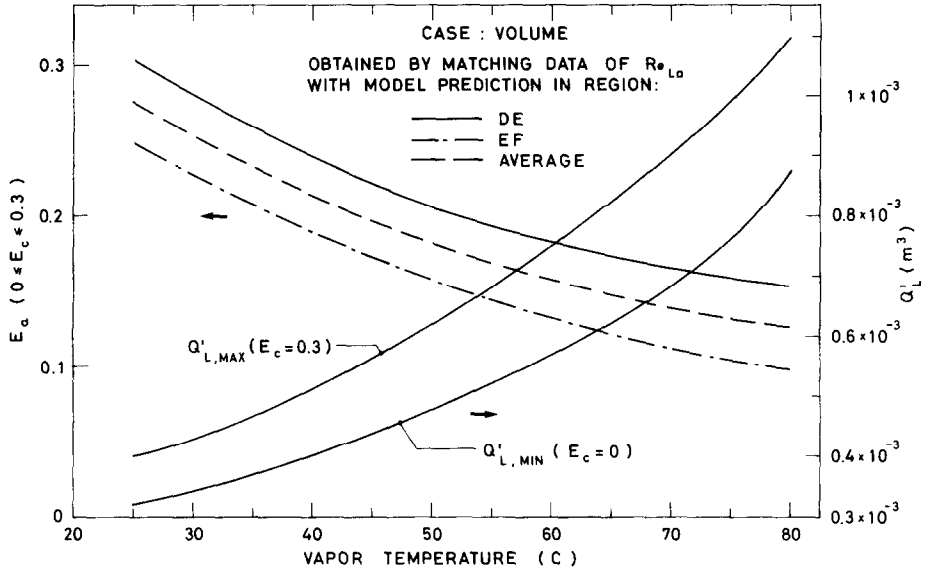

FIG. 11. Estimated entrainment and circulating volumes of the working fluid at the onset of flooding for the case Volume.

values of entrainments, and the results can be compared with data of the thermal blocking heat transfer rates as illustrated in Fig. 15. Note that by comparing the results of Figs. 10 and 13 there is essentially no difference in the prediction of flooding heat transfer rates at different entrainment values; but there is a significant and important difference in the prediction of the circulating working fluid volumes at flooding. This difference manifests itself clearly in Fig. 15 as may be seen by comparing the results with those of Fig. 12. The prediction of the experimental data can be achieved only with a non-zero value of the entrainment for all values of Q'_L in the range from $Q'_{L,MIN}$ to $Q'_{L,MAX}$. Moreover, high values of the circulating working fluid volumes require quite high values of entrainments to achieve a good prediction of data. As discussed previously, the actual value of Q'_L should be somewhere between $Q'_{L,MIN}$ and $Q'_{L,MAX}$ which, when compared with the results in Fig. 12 for the case Volume, implies that the case of ΔT Constant is not as suitable for predicting the thermally blocked heat transfer rates.

It should be noted in Fig. 15 that the lowest value of Q'_L and entrainment values of $E_a = E_c = 0.15$ tend to produce a flattening of Re_{La} at higher temperatures. To investigate this effect more thoroughly, shown in Fig. 16 is a study of the effect of some limiting values of entrainments on the Re_{La}-vapor temperature

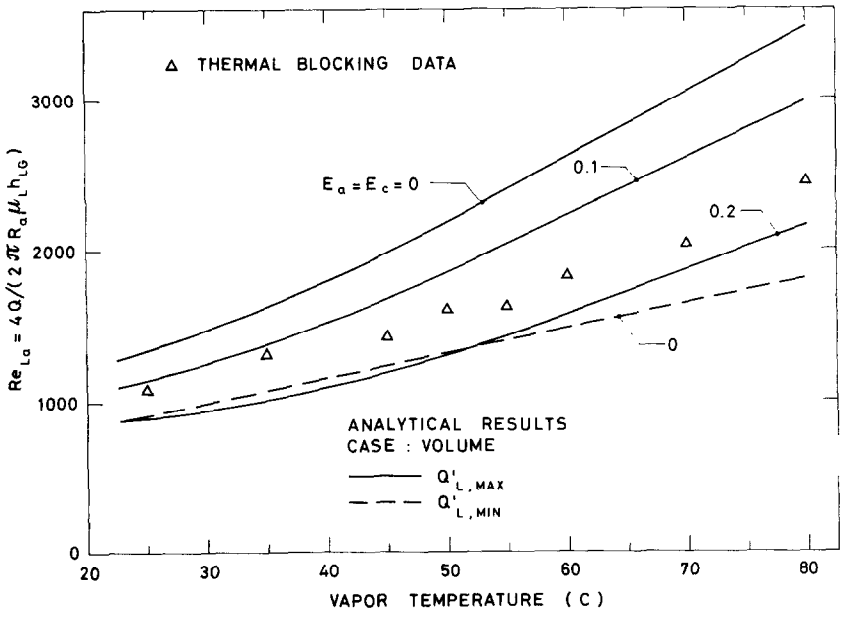

FIG. 12. Relationship between the experimental data of thermal blocking heat transfer rates and model predictions of the dryout heat transfer rates for the case Volume.

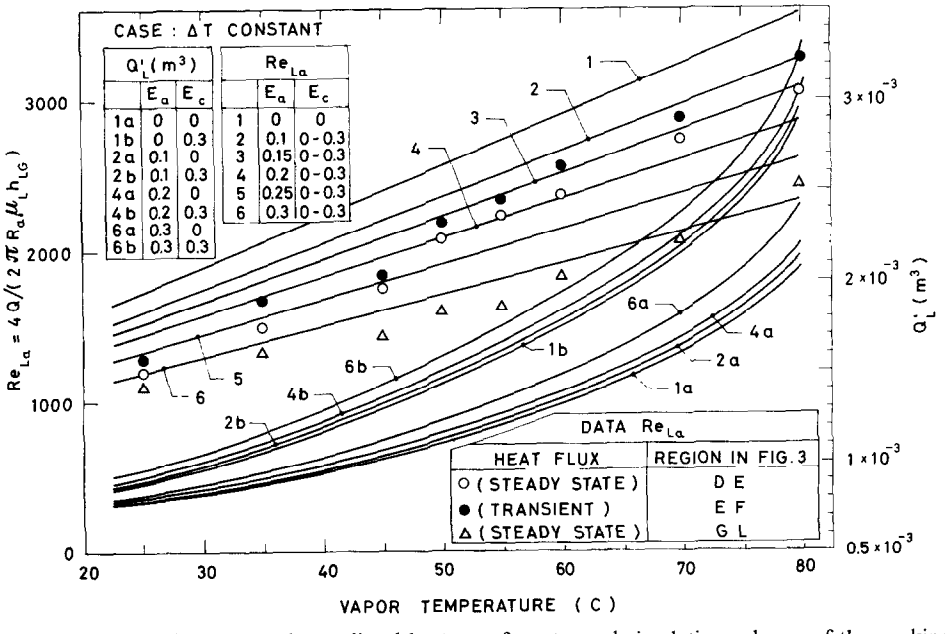

FIG. 13. Relationship between the predicted heat transfer rates and circulating volumes of the working fluid at flooding with the vapor temperature for different entrainments for the case ΔT Constant.

relationships at the dryout for the two cases of Table 1 and $Q'_{L,MIN}$ corresponding to Figs. 11 and 14. The conclusion from this figure is that a low value of Q'_L and the entrainment of liquid in the vapor core may not only produce a flattening noted above, but also a maximum in Re_{La}. Moreover, this effect is more pronounced for the higher entrainment values in the condenser. Note, however, that in the model the entrainment is specified as an independent parameter and that the maximum in Re_{La} may not exist.

In concluding this section on the modeling and analysis of data, it should be noted that the prediction of the thermally blocked heat transfer rates of the experimental thermosyphon was modeled only by the dryout in the evaporator and not with the simultaneous occurrence of a new flooding state in the thermosyphon as evidenced by the interpretation of the data. The present model is, clearly, too simple to be able to predict these simultaneous processes and has required, in effect, the elimination of the liquid from the pool of the evaporator at the occurrence of the flooding condition for the subsequent utilization

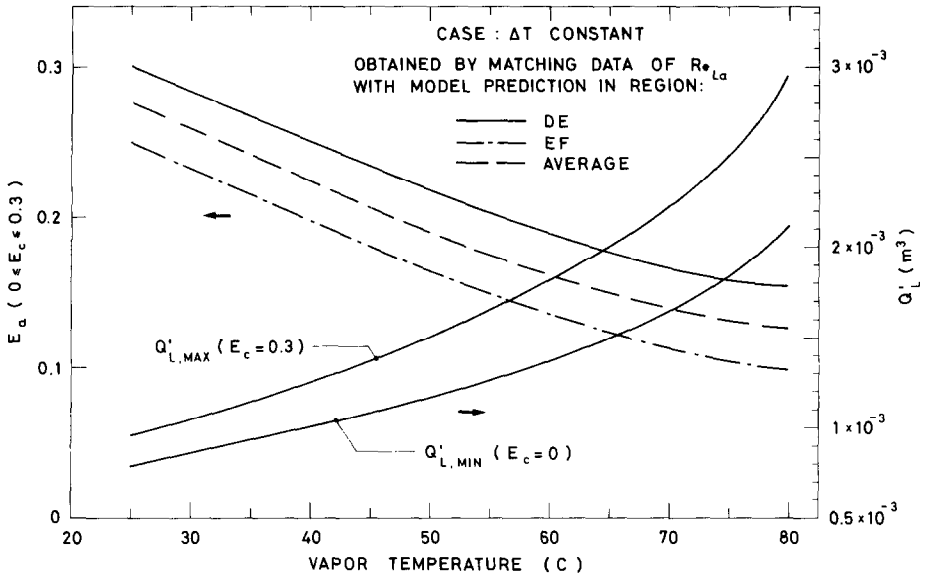

FIG. 14. Estimated entrainment and circulating volumes of the working fluid at the onset of flooding for the case ΔT Constant.

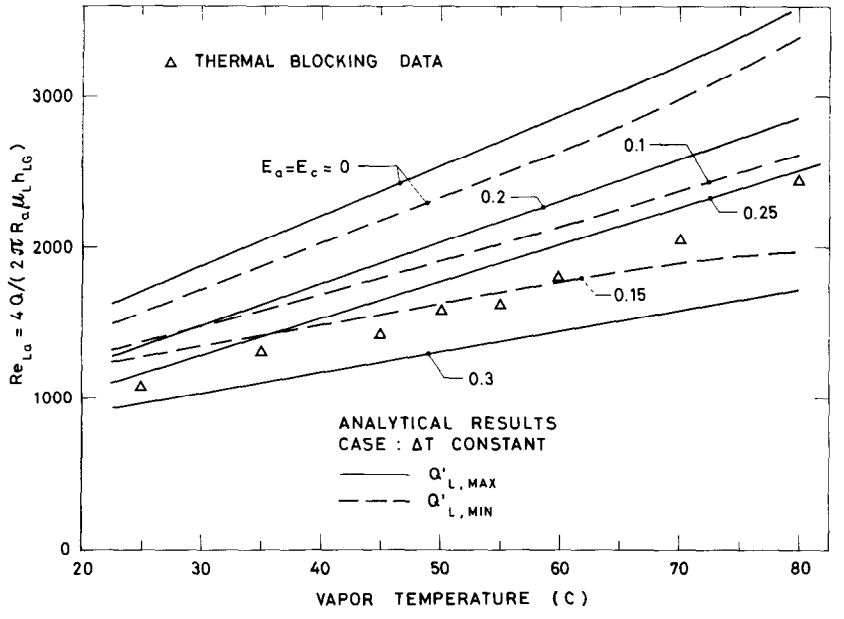

FIG. 15. Relationship between the experimental data of thermal blocking heat transfer rates and model predictions of the dryout heat transfer rates for the case ΔT Constant.

of the model in order to achieve a correspondence between the predicted dryout and the experimental thermally blocked heat transfer rates.

5. SUMMARY AND CONCLUSIONS

Experiments were conducted with Freon-11 in a closed two-phase thermosyphon with imposed heating and cooling fluid inlet temperatures in the evaporator and condenser. By increasing the temperature difference between the heating and cooling fluids it was discovered that the thermosyphon may exhibit different operational modes depending on this temperature difference. With an increasing heat transfer rate the thermosyphon at first exhibited a maximum heat transfer carrying capacity which was identified with the flooding heat transfer limit. Beyond this heat transfer limit the thermosyphon operation reverted to a new steady state with a lower heat transfer rate. This latter state was identified as the thermal blocking heat transfer limit, since any further increase in the temperature difference between the heating and cooling fluids did not produce a further change in the heat transfer capacity of the working fluid in the thermosyphon. The value of the thermal blocking heat transfer rate lower than that prior to the transition to

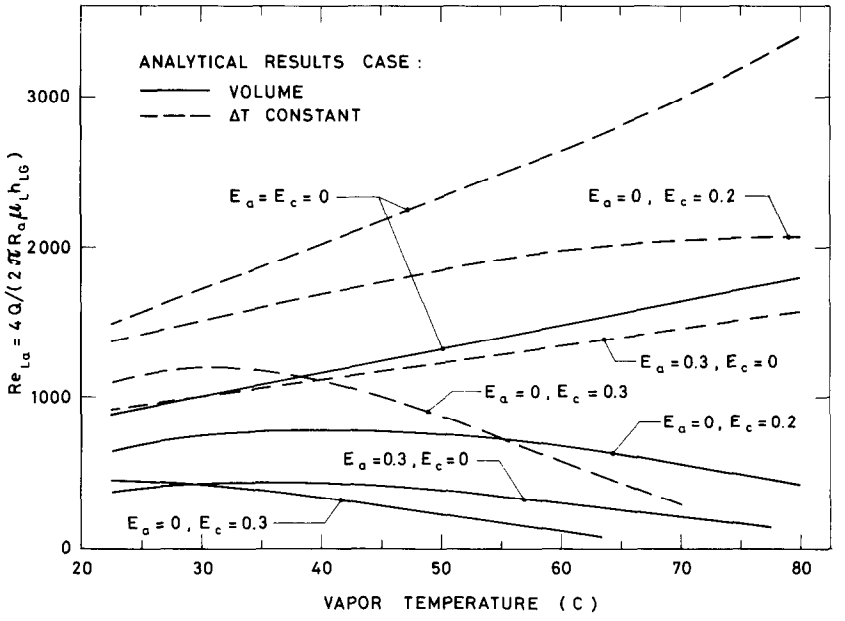

FIG. 16. Predicted dryout heat transfer rates for low values of the circulating working fluid volumes for the cases of Volume and ΔT Constant.

this state (flooding) was attributed to the simultaneous occurrence of the dryout in the evaporator and the establishment of a new flooding state in the adiabatic region. This resulted from the transfer of liquid from the evaporator to the condenser during the transient non-equilibrium process from the flooding state to that of the thermally blocked state. In the thermally blocked state the thermosyphon exhibited higher amplitude pressure oscillations and upon a decrease in the temperature difference of the heating and cooling fluids it reverted smoothly to the normal operation at a lower heat transfer rate.

The operation of the thermosyphon at different working fluid temperatures was modeled by a lumped parameter model which accounts for different geometric configurations of the evaporator and condenser regions, and includes the effect of the liquid droplet entrainment in the vapor cores of these regions. The model predictions of the flooding heat transfer rates was first verified with the uniform diameter thermosyphon data using water and methanol as working fluids. The prediction of flooding heat transfer rates prior to the change of state to the thermally blocked condition of the present experimental investigation was also shown to be very reasonable with the expected values of entrainment in the thermosyphon. By assuming a minimum and maximum value of the entrainment, the model was then used to predict the dryout heat transfer limits and the predictions were compared with the thermally blocked heat transfer data. This comparison turned out to be very reasonable if the model employs a small, but nonzero, value of the entrainment in the vapor core.

The imposed convection boundary conditions in the evaporator and condenser of a thermosyphon demonstrated that the thermosyphon may exhibit the operational modes which are different from the boundary condition of the imposed heat transfer rate to the evaporator. The lumped parameter modeling of the thermosyphon demonstrated not only its utility in modeling the experimental observations but also its efficiency and flexibility. As such, the model should prove to be a very useful tool for the prediction of thermosyphon performance with different geometries, boundary conditions and working fluids.

Acknowledgements—The authors wish to thank the Progetto Finalizzato Energetica, CNR-ENEA, for financing the construction of the experimental facility. Special thanks are due to Mr M. Celestino for the help given in conducting the experimental studies.

REFERENCES

1. B. S. Larkin, An experimental study of the two-phase thermosyphon tube, *Trans. Can. Soc. Mech. Engrs* **14**(B-6), 1–8 (1971).
2. Y. Lee and U. Mital, A two-phase closed thermosyphon, *Int. J. Heat Mass Transfer* **15**, 1695–1707 (1972).
3. H. Kusuda and H. Imura, Boiling heat transfer in an open thermosyphon, *Bull. J.S.M.E.* **16**, 1723–1740 (1973).
4. R. K. Sakhuya, Flooding constraint in wickless heat pipes. Paper ASME 73-WA/HT-7 (1973).
5. F. E. Andros and L. W. Florschuetz, The two-phase closed thermosyphon: an experimental study with flow visualization. In *Two-phase Transport and Reactor Safety*, Vol. IV, pp. 1231–1267. Hemisphere, New York (1978).
6. M. K. Bezrodnyi, The upper limit of maximum heat transfer capacity of evaporative thermosyphons, *Teploenergetica* **25**, 63–66 (1978).
7. M. K. Bezrodnyi, S. N. Faynzilberg and Ye. A. Kon-

drusik, Investigation of the maximum heat transfer in annular two-phase thermosyphons, *Heat Transfer—Sov. Res.* **12,** 119–123 (1980).
8. M. K. Bezrodnyi and S. S. Volkov, Study of hydrodynamic characteristics of two-phase flow in closed thermosyphons. In *Advances in Heat Pipe Technology*, pp. 115–123. Pergamon Press, Oxford (1981).
9. N. Nguyen-Chi and M. Groll, Entrainment or flooding limit in a closed two-phase thermosyphon. In *Advances in Heat Pipe Technology*, pp. 147–162. Pergamon Press, Oxford (1981).
10. T. Fukano, S. J. Chen and C. L. Tien, Operating limits of the closed two-phase thermosyphon, *Proc. ASME/JSME Thermal Engng Conf.*, Vol. I, pp. 95–101 (1983).
11. T. Fukano, K. Kadoguchi and C. L. Tien, Oscillation phenomena and operating limits of the closed two-phase thermosyphon, *Proc. 8th Int. Heat Transfer Conf.*, Vol. 5, pp. 2325–2330 (1986).
12. C. Casarosa, F. Fantozzi and E. Latrofa, Bloccaggio termico di un termosifone bifase operante con condizioni di scambio imposte, *41 Congresso Nazionale ATI*, Sezione VII, pp. 119–131 (1986).
13. C. Casarosa, F. Fantozzi, E. Latrofa and E. Martorano, Limite per flooding al transporto assiale di potenza termica in un termosifone bifase, *40 Congresso Nazionale ATI*, Sezione V, pp. 397–414 (1985).
14. C. P. Liu, G. E. McCarthy and C. L. Tien, Flooding in vertical gas–liquid countercurrent flow through multiple short paths, *Int. J. Heat Mass Transfer* **25,** 1301–1312 (1982).
15. D. Bharathan and G. B. Wallis, Air–water countercurrent annular flow, *Int. J. Multiphase Flow* **9,** 349–366 (1983).
16. C. L. Tien and K. S. Chung, Entrainment limits in heat pipes, *Proc. 3rd Int. Heat Pipe Conf.*, Palo Alto, pp. 36–40 (1978).
17. F. Dobran, Steady state characteristics and stability thresholds of a closed two-phase thermosyphon, *Int. J. Heat Mass Transfer* **28,** 949–957 (1985).
18. F. Dobran, Parametric study and transient analysis of closed two-phase thermosyphons with distributed diameters and liquid entrainment, in preparation.
19. F. Dobran, Heat transfer in an annular two-phase flow, *J. Heat Transfer* **107,** 472–476 (1985).
20. J. G. Reed and C. L. Tien, Modeling of the two-phase closed thermosyphon, *J. Heat Transfer* **109,** 722–730 (1987).
21. W. M. Rohsenow, J. P. Hartnett and E. N. Ganic (Editors), *Handbook of Heat Transfer Fundamentals*, p. 11.18. McGraw-Hill, New York (1985).
22. M. Ishii and K. Mishima, Liquid transfer and entrainment correlation for droplet-annular air flow, *Proc. 7th Int. Heat Transfer Conf.*, Vol. 5, pp. 307–312 (1982).

ETUDE EXPERIMENTALE ET MODELE ANALYTIQUE D'UN THERMOSIPHON DIPHASIQUE AVEC DES CONDITIONS DE CONVECTION AUX LIMITES

Résumé—Un thermosiphon diphasique fermé opérant avec du R-111 et des conditions convectives aux limites sur les surfaces chaudes et froides est étudié expérimentalement et modélisé analytiquement pour les températures du fluide. On observe différents modes opératoires qui dépendent de la différence de température entre chauffage et refroidissement du fluide. Un accroissement de cette différence produit d'abord un taux de transfert thermique maximal identifiable à la limite d'engorgement. Au delà de ce point, le fonctionnement du thermosiphon se renverse en un état stationnaire en passant par un mécanisme transitoire hors d'équilibre. Le nouvel état stationnaire, identifié avec la condition de blocage thermique, produit un transfert plus faible et il correspond à l'existence simultanée (1) d'un nouvel état d'engorgement près de la sortie de la section adiabatique et (2) d'un assèchement dans l'évaporateur qui résulte du transfert du liquide de l'évaporateur vers le condenseur, ce qui conduit à la condition de blocage thermique. Les modes opératoires limitants du thermosiphon sont modélisés par un modèle qui tient compte des différentes configurations géométriques et de l'entrainement du liquide dans la vapeur. Une comparaison entre les flux de chaleur prédits et expérimentaux, avant et pendant la condition de blocage thermique, montre l'utilité du modèle pour prédire les mécanismes thermohydrauliques complexes dans un thermosiphon.

EXPERIMENTELLE UND ANALYTISCHE UNTERSUCHUNGEN AN EINEM GESCHLOSSENEN ZWEIPHASEN-THERMOSYPHON BEI KONVEKTIVEN RANDBEDINGUNGEN

Zusammenfassung—Ein mit Kältemittel R11 betriebener geschlossener Zweiphasen-Thermosyphon wurde bei konvektiven Randbedingungen an der beheizten und gekühlten Oberfläche experimentell untersucht und analytisch mit einem Modell mit verteilten Parametern für unterschiedliche Arbeitsmitteltemperaturen nachgebildet. Der Thermosyphon weist verschiedene Betriebszustände auf, die von der Temperaturdifferenz zwischen dem Heiz- und Kühlfluid abhängt. Eine Zunahme dieser Temperaturdifferenz ruft zuerst ein Maximum der übertragenen Wärme hervor, das gleichzusetzen ist mit der Wärmeübertragungsgrenze beim "Flooding". Oberhalb dieser Grenze kehrt der Thermosyphon über einen transienten Vorgang zu einem neuen, stationären Zustand zurück. Dieser neue stationäre Zustand, als "Thermal Blocking" bezeichnet, zeigt ein niedrigeres Wärmeübertragungsvermögen und wird zurückgeführt auf die gleichzeitige Existenz von: (1) "Flooding" in der Nähe oder am Ausgang des adiabaten Bereichs, (2) Austrocknen des Verdampfers, der aus einem Flüssigkeitstransport vom Verdampfer in den Kondensator während des transienten Vorgangs resultiert. Die Betriebsgrenzen des Thermosyphons werden durch ein Modell mit verteilten Parametern nachgebildet, das verschiedene geometrische Anordnungen und Entrainment von Flüssigkeit im Dampf zuläßt. Ein Vergleich zwischen berechnetem und gemessenem Wärmeübergang vor und während des "Thermal-Blocking" zeigt die Nützlichkeit des Modells zur Berechnung komplexer thermohydrodynamischer Vorgänge in einem Thermosyphon.

ЭКСПЕРИМЕНТАЛЬНОЕ ИССЛЕДОВАНИЕ И АНАЛИТИЧЕСКОЕ МОДЕЛИРОВАНИЕ ЗАМКНУТОГО ДВУХФАЗНОГО ТЕРМОСИФОНА ПРИ ЗАДАННЫХ КОНВЕКТИВНЫХ ГРАНИЧНЫХ УСЛОВИЯХ

Аннотация—Проведено экспериментальное исследование замкнутого двухфазного термосифона, в котором в качестве рабочей жидкости используется фреон-11, а на нагреваемой и охлаждаемой поверхностях задаются конвективные граничные условия. Используя кусочные параметры для описания изменяющейся температуры рабочей жидкости, разработана аналитическая модель процесса. В зависимости от разности температур между нагревающей и охлаждающей жидкостями имели место различные режимы работы термосифона. При увеличении этой разности интенсивность теплопереноса сначала достигала максимума, который отождествляется с предельной величиной теплового потока при затоплении. Затем через нестационарное неравновесное состояние термосифон выходил на новый стационарный режим. В этом режиме, приравниваемом к возникновению условия тепловой блокировки, отмечается снижение теплопередающей способности из-за одновременного воздействия следующих факторов: (1) очередное затопление вблизи адиабатического участка или на выходе из него и (2) кризис теплообмена в испарителе в результате перетока жидкости в конденсатор, приводящий к появлению условия тепловой блокировки. Предельные рабочие режимы термосифона моделировались с помощью кусочных параметров, учитывающих различную геометрию аппарата и унос жидкости паром. Сравнение расчетных и экспериментальных значений интенсивности теплопереноса до тепловой блокировки и во время ее показало, что предложенная модель может использоваться для расчета сложных термогидродинамических процессов, происходящих в термосифоне.